ACS APPLIED MATERIALS & INTERFACES

www.acsami.org

Research Article

Comparative Determination of Cytotoxicity of Sub-10 nm Copper Nanoparticles to Prokaryotic and Eukaryotic Systems

Savanna S. Skeeters, Ana C. Rosu, Divyanshi, Jing Yang, and Kai Zhang*

Cite This: *ACS Appl. Mater. Interfaces* 2020, 12, 50203−50211

Read Online

ACCESS | Metrics & More | Article Recommendations | Supporting Information

ABSTRACT: Copper nanoparticles demonstrate antibacterial activity, but their toxicity to eukaryotic systems is less understood. Here, we carried out a comparative study to determine the biocompatibility and cytotoxicity of sub-10 nm copper nanoparticles to a variety of biological systems, including prokaryotic cells (*Escherichia coli*), yeast, mammalian cell lines (HEK293T, PC12), and zebrafish embryos. We determined the bearing threshold for the cell-death-inducing concentration of copper nanoparticles by probing cell growth, viability, as well as embryological features. To exclude the partial toxicity effect from the remnant reactants, we developed a purification approach using agarose gel electrophoresis. Purified CuONP solution inhibits bacterial growth and causes eukaryotic cell death at 170 and 122.5 ppm (w/w) during the 18 h of treatment, respectively. CuONP significantly reduces the pigmentation of retina pigmented epithelium of zebrafish embryos at 85 ppm. The cytotoxicity of CuONP in eukaryotic cells could arise from the oxidative stress induced by CuONP. This result suggests that small copper nanoparticles exert cytotoxicity in both prokaryotic and eukaryotic systems, and therefore, caution should be used to avoid direct contact of copper nanoparticles to human tissues considering the potential use of copper nanoparticles in the clinical setting.

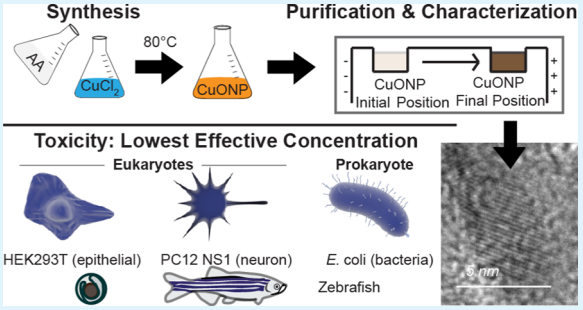

KEYWORDS: *copper nanoparticles, green synthesis, cytotoxicity, prokaryotic, eukaryotic, zebrafish embryos*

INTRODUCTION

Metallic nanoparticles have attracted investigators from a number of research fields, including physics, chemistry, material sciences, and biological sciences, owing to their advantages in catalysis,[1] biosensing,[2−7] and pharmaceutics.[8−10] As the size of the nanoparticle decreases, its increased surface-area-to-volume ratio changes the physical, optical, and biological properties of the particle. Of particular interests are the inert metallic nanoparticles (silver, gold, and copper). Because surface plasmon resonance in silver and gold results in enhanced light absorption and scattering in the visible light spectrum, both silver and gold nanoparticles have been widely used in biological imaging and sensing. In addition, silver nanoparticles have been widely studied for their cytotoxicity toward bacterial and mammalian cells.[11,12] However, the suboptimal stability limits the application of silver nanoparticles in biological systems.

Being more stable than silver, copper has thus gained considerable attention for its antimicrobial properties. Multiple studies have shown that copper nanoparticles exert cytotoxicity like silver nanoparticles.[13−16] Indeed, solid copper and copper films have been used to create sterile surfaces on countertops, catheters, and cotton.[17,18] Copper nanoparticles of 20−500 nm exhibit toxicity toward multidrug-resistant bacteria and biofilms.[19−21] Because the reactivity of metals can increase as the size of the nanoparticle decreases,[11,12] it is expected that smaller copper nanoparticles could be more effective in their biological applications. Unfortunately, currently developed synthetic routes for copper nanoparticles mostly generate particles larger than 10 nm.[1] Production of sub-10 nm copper particles has been challenging until recently. For example, the Wu group reported an assay of synthesizing small copper nanoparticles (sub-2 nm in diameter) without the use of extreme temperatures or pressures.[22] These sub-10 nm copper nanoparticles show great potential in biomedical and engineering, particularly in bioimaging,[23] biosensing,[24] production of conductive nanoink,[25] electrode design,[26] catalysis,[27] and photovoltaics.[28] The convenient synthetic approach and the resulting stable particle products inspire us to further characterize the physicochemical and biological properties of sub-10 nm copper nanoparticles. Indeed, the antibacterial effects of embedded small copper nanoparticles (2.5 nm),[29] as well as the cytotoxicity of larger (25−100 nm) copper nanoparticles to mammalian cell lines,[30] have been reported. However, comparative studies on the cytotoxicity of the sub-10

Received: June 17, 2020
Accepted: October 16, 2020
Published: October 30, 2020

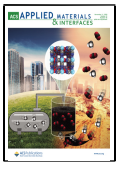

https://dx.doi.org/10.1021/acsami.0c11052
ACS Appl. Mater. Interfaces 2020, 12, 50203−50211

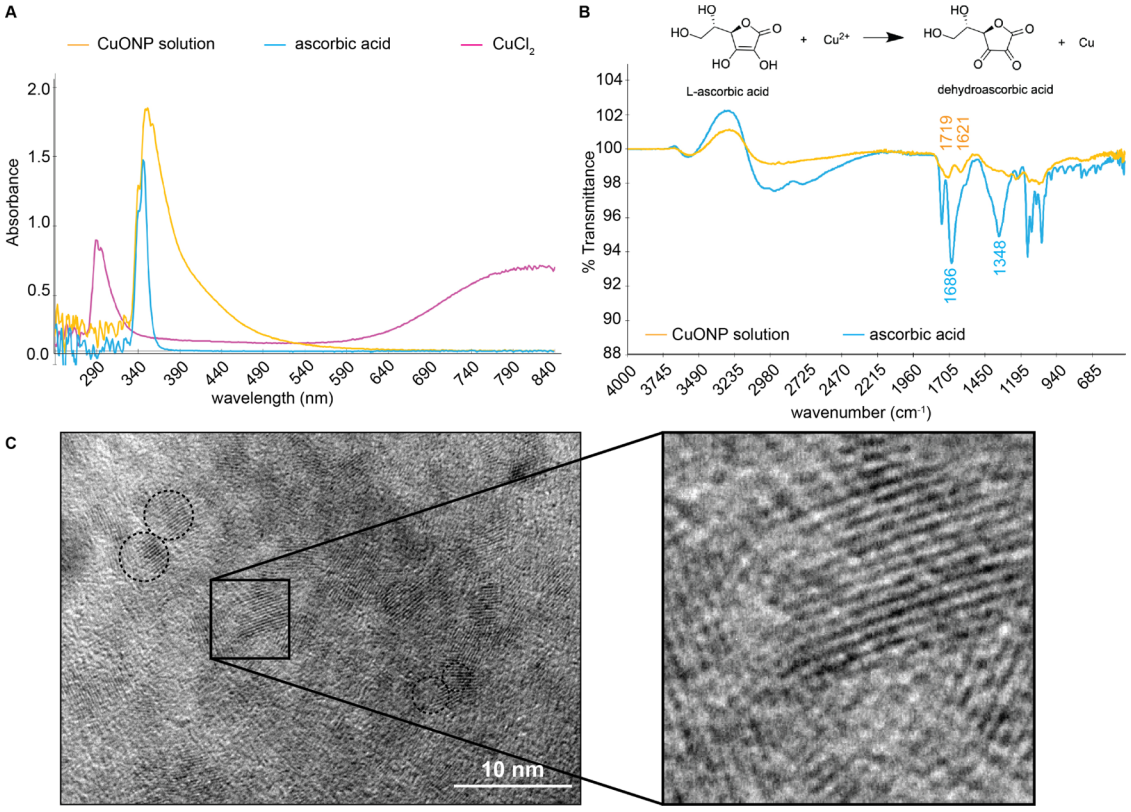

Figure 1. Characterization of synthesized copper oxide nanoparticles. (A) UV/vis absorbance of reactants (600 mM L-ascorbic acid and 10 mM $CuCl_2$) compared to that of the product after heat. A 1:64 diluted CuONP solution (approximately 5 ppm) was used. (B) FT-IR spectrum of untreated 600 mM L-ascorbic acid compared to that of the CuONP solution (300 ppm) with an inlaid reaction scheme. (C) Transmission electron microscopy (TEM) imaging of the CuONP solution showing nanoparticles of varied shapes and sizes less than 10 nm with crystalline copper lattices (scale bar, 10 nm).

nm copper nanoparticles in prokaryotic and eukaryotic systems remain limited.

In contrast to the antibacterial effect of copper nanoparticles in isolation, the examination of the antibacterial effect within eukaryotic hosts requires a comparative, parallel study on the toxicity in both bacterial and eukaryotic systems, which remains unavailable in the literature.

Thus, in this work, we set out to determine the biocompatibility and selectivity of the antimicrobial effects of sub-10 nm copper nanoparticles between multiple eukaryotic and prokaryotic systems. Here, we define biocompatibility as the concentration of copper nanoparticles that the eukaryotic system (host) can withstand (safe bearing level). We define selectivity as the differential toxicity effect of copper nanoparticles on bacteria and eukaryotic cells (effective bacterial killing). An excellent antibacterial reagent would ideally have high biocompatibility and high selectivity. In this work, we used HEK293T and PC12 cultured cells as representative eukaryotic model systems and *Escherichia coli* as representative bacteria. We also determined the toxicity of CuONP in yeast, a eukaryotic system with the cell wall. We further determined the effects of sub-10 nm CuONP on developing zebrafish embryos, particularly on the pigmentation of retina pigmented epithelium, a crucial tissue for eye development. The goal of this work is to provide a comparative study on the biological effects of sub-10 nm copper particles on multiple systems from bacteria, yeast, mammalian cells, and live zebrafish embryos.

RESULTS AND DISCUSSION

Synthesis and Characterization of Copper/Copper Oxide Nanoparticles. Copper nanoparticles were synthesized by following the previous studies.[22,29] Briefly, $CuCl_2$ was reduced by L-ascorbic acid, which also acts as the surfactant, followed by incubation in the convection oven at 80 °C for 22 h. UV−vis spectroscopy of the resulting solution (Figure 1A) shows the appearance of an absorption peak at around 350 nm, as well as the disappearance of the 640−840 nm absorption from the $CuCl_2$ solutions, indicating the formation of copper/copper oxide nanoparticles (referred to as CuONPs). It was postulated that the reduction of Cu^{2+} to Cu^0 by L-ascorbic acid generates a semi-dehydroascorbic acid intermediate.[22] We further outlined a possible mechanism for this reaction: deprotonated L-ascorbic acid coordinates with Cu^{2+} and allows for a two-electron transfer process to produce dehydroascorbic acid and Cu^0 (Figure 1B). Consumption of ascorbic acid was confirmed by the disappearance of 950−1960 cm^{-1} peaks when we overlaid the Fourier transform infrared (FT-IR) spectra of the particle solution and pure ascorbic acid (Figure 1B).

The formation of the CuONP was further confirmed by electron microscopy (Figure 1C). Larger aggregates in the solution were removed by centrifugation, and the remaining supernatant was dried on the TEM grid before imaging. Representative copper/copper oxide particles are indicated by dashed circles in Figure 1C. The inset shows the crystalline lattice of the nanoparticles. Thus, we confirmed the successful

https://dx.doi.org/10.1021/acsami.0c11052
ACS Appl. Mater. Interfaces 2020, 12, 50203−50211

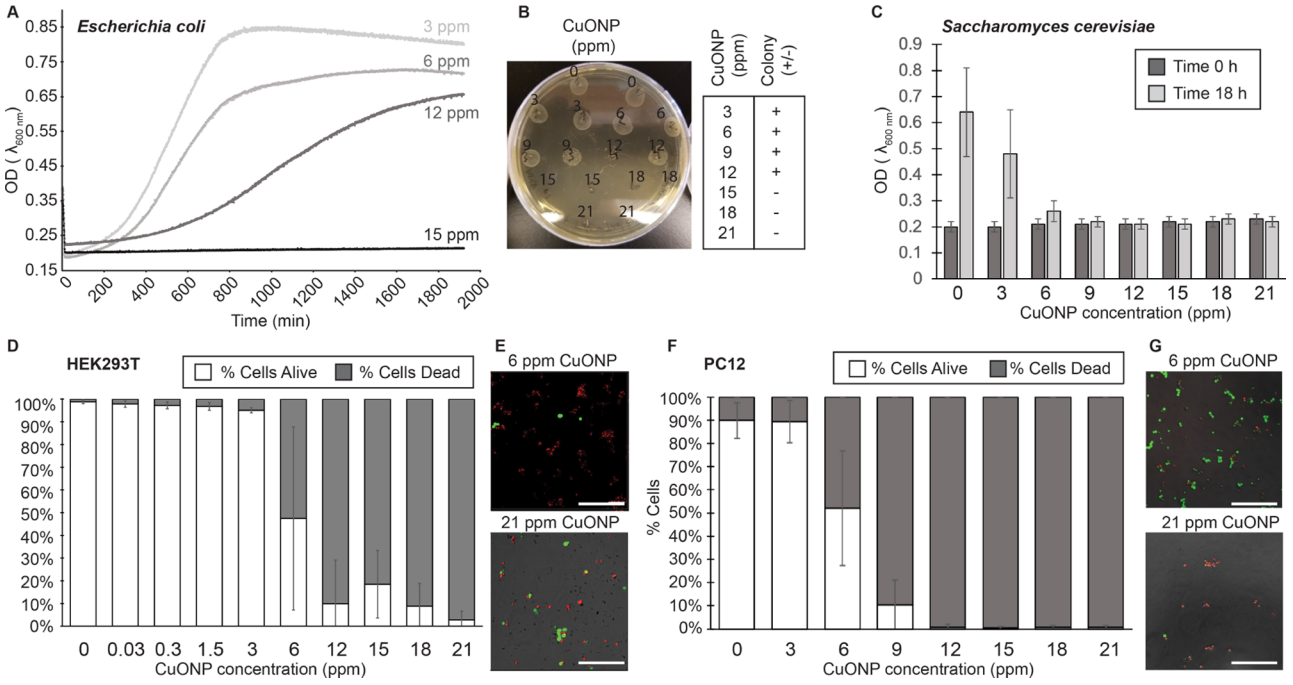

Figure 2. CuONP solution shows toxicity in bacteria, human kidney cells, and rat neuronal cell lines. (A) Growth curves for bacteria treated with the 3, 6, 12, or 15 ppm (w/w) unpurified CuONP solution. (B) Cells grown in the presence of unpurified CuONP in (A) were then plated on agar to determine the cell viability after long-term (33 h) exposure. Results are shown as (+) for the appearance of colonies and (−) for no colony formation. (C) The effect of unpurified CuONP on yeast growth was measured by OD at 600 nm (N = 3). (D) HEK293T cells were treated with the unpurified CuONP solution, and cell viability was determined by propidium iodide or PI (red fluorescence, staining dead cells) and calcein-AM (green fluorescence, staining live cells) (N = 3 except for the 6 and 12 ppm conditions where N = 5). (E) Representative staining images for (D). (F) PC12 cells were treated with the unpurified CuONP solution, and cell viability was determined by PI and calcein-AM staining. (G) Representative staining images for (F).

production of sub-10 nm CuONP. The estimated stock concentration of CuONP is 300 ppm (w/w).

Copper Nanoparticles Reduce the Growth Rate of Bacteria and Yeast and Cause Dose-Dependent Toxicity. Copper nanoparticles are well established as antimicrobial agents,[21] but the biotoxicity of sub-10 nm copper/copper oxide nanoparticles is yet to be characterized. To determine the biotoxicity of these small CuONP, we measured the growth curve of bacteria by titrating with different doses of particles. We first produced a starter culture by growing an ampicillin-resistant *E. coli* strain to the log phase in Lennox broth containing ampicillin. From this starter, solutions containing freshly synthesized CuONP (at 3, 6, 12, and 15 ppm, w/w) were inoculated and grown overnight in a plate reader at 37 °C with constant shaking and continuous measurement of optical density at 600 nm (Figure 2A). Cells in the 3 ppm CuONP solution showed typical growth curves, whereas those in the 6 ppm CuONP solution grew at a slower rate and did not reach the same endpoint stationary optical density. Cells in the 12 ppm CuONP solution grew significantly slower and reached lower endpoint optical density than that in the 6 ppm CuONP solution. Cells in the 15 ppm solution did not grow at all.

To determine whether the CuONP solution inhibited cell growth or caused cell death, we recovered the endpoint cells on marked LB plates supplemented with ampicillin. Ten microliters of cells were dropped on the plate, incubated overnight, and checked for colonies the following day. Cells in the 3−9 ppm CuONP solution consistently grew colonies. Cells in the 12 ppm solution grew colonies, but the size of the spread was far smaller than that of the 3−9 ppm group (Figure 2B). Cells in the 15−21 ppm CuONP solution never grew colonies. These results indicated that the copper oxide nanoparticles exert a bactericidal effect at concentrations greater than 12 ppm.

Next, we sought to understand whether this cytotoxicity was limited to bacteria or also affected the viability and growth of eukaryotes. First, we repeated the cell growth assay with *Saccharomyces cerevisiae* yeast cells by titrating with different doses of CuONP. Similar to the effect on bacterial growth, we observed a strong inhibition of cell growth when more than 6 ppm CuONP was incubated (Figure 2C). We then proceeded to determine the cytotoxicity of CuONP in mammalian cells by selecting two cell lines as the model systems: human embryonic kidney cells (HEK293T cell line) and rat neuronal cells (PC12 NS1). These two cell lines were selected because (1) they are commonly used in biomedical research, and (2) their biological makeup represents distinct eukaryotic cell types (epithelial and neuronal). Cell viability was determined by dual staining with calcein-AM (for live cells) and propidium iodide (for dead cells). In HEK293T cells, CuONP cytotoxicity began at as low as 6 ppm with nearly complete cell death by 21 ppm (Figure 2D,E). In PC12 cells, toxicity began at 6 ppm with nearly complete cell death at 12 ppm (Figure 2F,G). Therefore, this CuONP solution was not solely toxic to bacteria but also to rat and human cell lines.

It is well documented that Cu(II) could induce oxidative stress in bacteria and exert the toxicity effect.[31] Thus, we proceeded to determine whether the cytotoxicity in mammalian cells involves oxidative stress as well. To do this, we compared HEK293T cell death in a culture treated with CuONP or CuONP and 50 mM β-mercaptoethanol (BME), a

https://dx.doi.org/10.1021/acsami.0c11052
ACS Appl. Mater. Interfaces 2020, 12, 50203−50211

reducing agent. We expected that BME could partially rescue cell viability under an appropriate level of oxidative stress. Consistent with the previous result, CuONP (6 ppm) caused significant cell death as measured by propidium iodide staining. In the presence of 50 mM BME, however, we observed that more than half of the cell population was viable revealed by calcein-AM staining (Figure S2). As the concentration of CuONP increased, the rescuing effect of BME was less significant. This result suggests that the cytotoxicity of CuONP in mammalian cells also involves its capacity to induce oxidative stress.

Unreacted Reactants for the Synthesis of Copper Nanoparticles Cause Partial Toxicity in Bacteria and Mammalian Cells. Although we could successfully reproduce the previous synthetic route to generate sub-10 nm copper nanoparticles, we note that no purification step was developed in the previous work. Although the majority of physical and chemical properties of nanoparticles may not be affected by the remnant reactants, we could not ignore their contribution to cell toxicity. We first determined the remaining concentration of $CuCl_2$ by UV/vis spectroscopy. $CuCl_2$ has a broad absorption peak at 800 nm. This peak virtually disappeared in the final diluted CuONP solution. However, in concentrated CuONP solution, light scattering significantly broadens the CuONP absorption peak at 800 nm, which may artificially inflate the estimation of particle concentration. With this in mind, if none of the $CuCl_2$ was consumed in the reaction, the maximum possible concentration of $CuCl_2$ in a 21 ppm solution would be 0.7 mM (Figure S1). Based on the UV−vis absorption spectrum of the CuONP, we estimated that the remnant $CuCl_2$ concentration should be less than 0.1 mM, which should not cause significant cytotoxicity based on the dose-dependent study on $CuCl_2$ alone (Figure 3A). We also expected that unreacted L-ascorbic acid could partially cause cytotoxicity. When prepared in isolation, 5 mM L-ascorbic acid was sufficient to cause significant cell death (Figure 3A), which was assayed by calcein-AM/PI staining in HEK293T cells (Figure 3B). The partial contribution from the L-ascorbic acid should, therefore, be separated from that of CuONP alone.

Develop a Purification Strategy for Copper Nanoparticles with Agarose Gel Electrophoresis. Next, we aimed to quantify the cellular toxicity of purified sub-10 nm nanoparticles. However, we found that traditional purification assays, such as chromatography and ultracentrifugation, could not be used to purify the sub-10 nm copper particles due to the small particle size. Additionally, extractions using harsh solvents could leave behind toxic components, convoluting the direct killing efficiency of the copper oxide nanoparticles. To address these challenges, inspired by the previous work of gold nanoparticle purification,[32,33] we developed a purification strategy based on agarose gel electrophoresis. While the copper nanoparticles themselves are not charged, we speculated that the surfactant could provide enough negative charge to allow for particle movement in an electric field (Figure 4A).

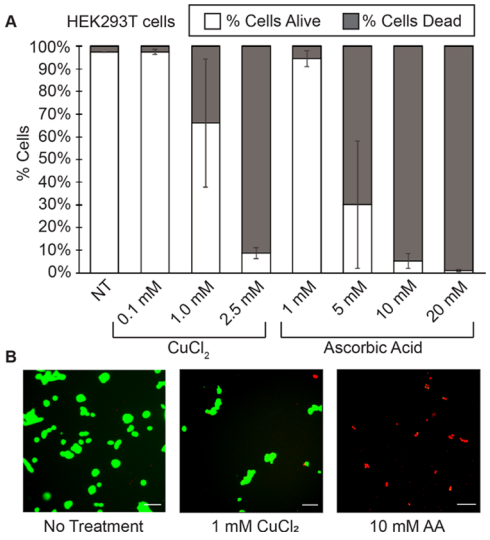

Figure 3. Unpurified CuONP solution has additional toxicity from unreacted reactants. (A) HEK293T cells were treated with the solution of each reactant at low concentrations relative to the starting concentration and cell viability was determined by PI (red, dead cells) and calcein-AM (green, live cells) staining. (B) Representative images of PI and calcein-AM overlay.

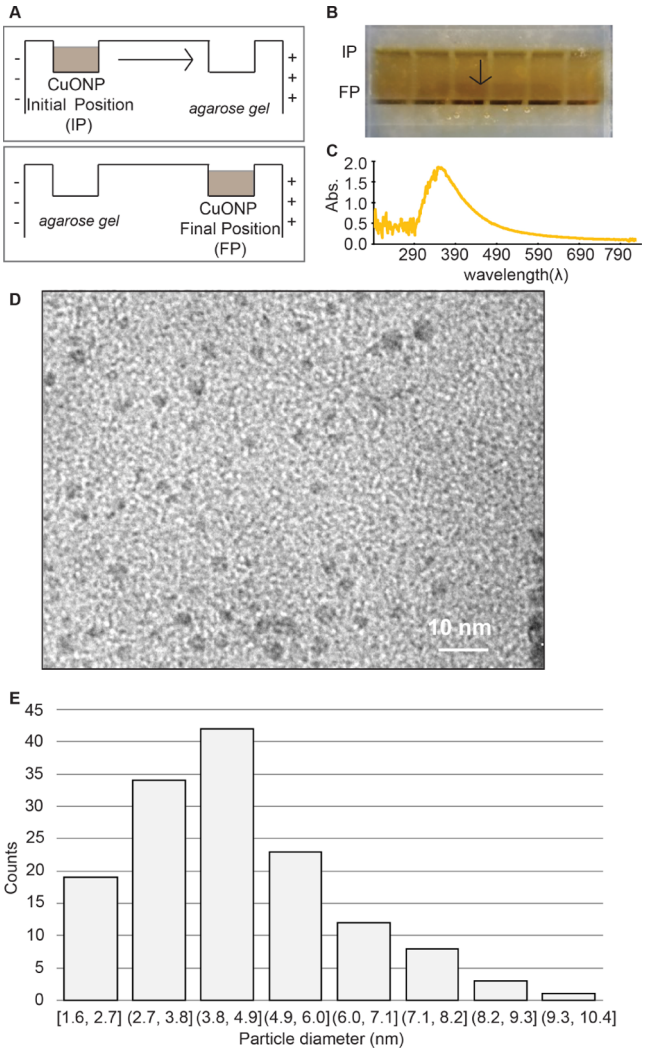

Figure 4. Characterization of purified CuONP. (A) Schematic depicting purification of CuONP from solution in an agarose gel. (B) Photograph of the CuONP solution that has traveled from the initial position to the final position, where CuONPs were ready to be collected. (C) UV/vis spectrum of purified CuONP. (D) TEM images of purified CuONP. (E) Quantification of the size of the CuONP from TEM imaging.

https://dx.doi.org/10.1021/acsami.0c11052
ACS Appl. Mater. Interfaces 2020, 12, 50203−50211

To test this idea, we prepared 2% agarose gel in 40 mM Tris-acetate buffer (TA buffer) and set two wells at the initial position (IP) and final position (FP), which were located approximately 2 cm apart (Figure 4B). The crude CuONP solution containing unreacted $CuCl_2$ and L-ascorbic acid was loaded into the well in IP. The nanoparticles, which were tinted brown from Cu^0, could be readily visualized through the opaque agarose gel. When an electric field was applied, as expected, nanoparticles collectivel moved toward the positive electrode, indicating that surfactants provided negative charges to the particle surface. When traveling to the final position (FP), the dark band containing particles was collected by a long pipet tip. The collection should consist of CuONP primarily because L-ascorbic acid and $CuCl_2$ should not travel in the same band. The solution was then dried in a rotary evaporator, massed, and resuspended in diethyl pyrocarbonate (DEPC)-treated water at a concentration of 2000 ppm (w/w). UV/vis spectroscopy confirmed the presence of the nanoparticles in the purified solution, as evidenced from the peak at around 380 nm (Figure 4C).

TEM images of purified CuONP showed that most particles are spherical (Figure 4D), with an average diameter of approximately 5 nm (Figure 4E). To determine whether particle aggregation could occur, we measured the hydrodynamic radius of these particles using dynamic light scattering. Purified CuONP at 2000 ppm showed a hydrodynamic radius of 648.2 nm, significantly larger than the size of single particles. Intriguingly, the diluted sample showed a reduction in the average hydrodynamic radius. At 2.5 ppm, the hydrodynamic radius was reduced to 142.5 nm (Table S1). This result indicates that although particle agglomeration occurs, they do not form a large, hard agglomerate but could dissociate into stable, smaller clusters. Indeed, the average ζ-potential of purified CuONP at 2.5 ppm was −29.7 mV, indicating that a stable structure with negative surface charges, consistent with the migration direction in the gel electrophoresis experiment (Table S2).

Determine the Cytotoxicity of Purified Nanoparticles. The purified nanoparticles were then tested for their toxicity in bacteria and human kidney cells. Ampicillin-resistant *E. coli* cultures were treated with 8.5, 42.5, 85, 122.5, and 170 ppm of purified CuONP solutions. As a control, cells were also treated with TA buffer at an equivalent volume of the corresponding CuONP solutions (1, 5, 10, 15, and 20% v/v). Cells experienced toxicity at the 170 ppm CuONP treatment but in none of the buffer-treated conditions, indicating that the toxicity seen was the direct result of the isolated nanoparticles (Figure 5A).

Isolated CuONP toxicity was then investigated in human cells. HEK293T cells were also treated with 8.5, 42.5, 85, 122.5, and 170 ppm purified CuONP solutions or TA buffer. Calcein-AM and propidium iodide staining showed that HEK293T cells experienced about 20% death at 122.5 ppm, and the death percentage increased to 40% at 170 ppm purified CuONP (Figure 5B). To better understand the effect of CuONPs on the metabolism of mammalian cells, we used the MTS assay (MTS tetrazolium-based protocol) to measure the population of metabolically active cells based on the activity of NAD(P)H-dependent dehydrogenase. Consistent with the live/dead cell staining results, HEK293T cells showed decreased metabolic activity as the concentration of CuONP increased from 8.5 to 170 ppm in a dose-dependent manner.

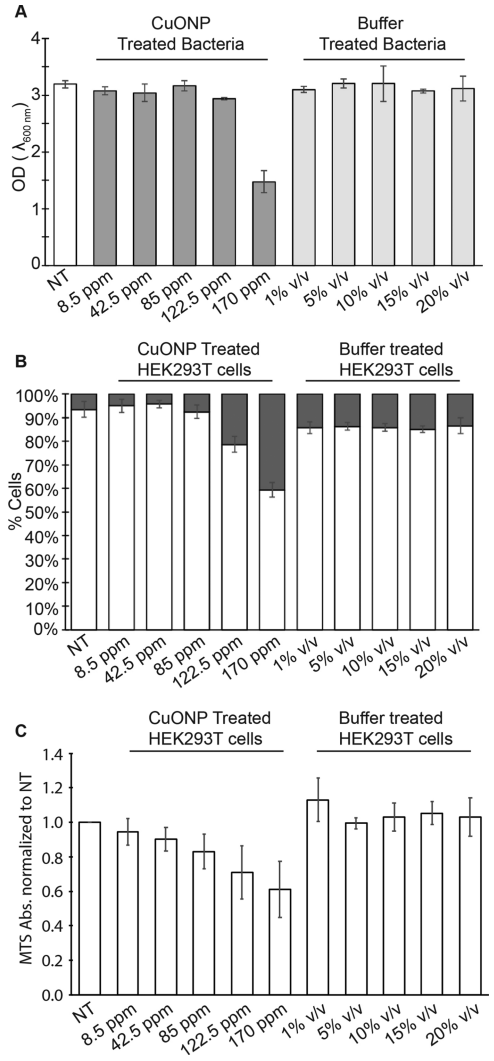

Figure 5. Determination of the cytotoxicity of purified CuONP to mammalian cells. (A) Endpoint growth for bacteria treated with purified CuONP or an equal volume of buffer ($N = 3$). (B) HEK293T cells were treated with either purified CuONP or buffer, and cell viability was determined by propidium iodide (dead cells) and calcein-AM (live cells) staining ($N = 3$). (C) HEK293T cells were treated with either purified CuONP or buffer, and cell proliferation was determined via a 3-(4,5-dimethylthiazol-2-yl)-5-(3-carboxymethoxyphenyl)-2-(4-sulfophenyl)-2H-tetrazolium (MTS) assay ($N = 3$).

TA buffer alone had no significant effects on the metabolic activity of HEK293T cells (Figure 5C).

CuONP Reduces Pigmentation of Retina Pigmented Epithelium in Zebrafish Embryos. To determine whether sub-10 nm CuONP exerts toxicity in living organisms, we set out to probe the effect of CuONP on early embryonic development in zebrafish (Figure 6A). At 24 h post fertilization (hpf), we manually removed the chorion from the embryos and treated embryos with 85 ppm CuONP. At 48 hpf, the development of retina pigmented epithelium (RPE) became evident in the majority (83.6%) of the untreated control embryos, judged by pigmentation in the RPE (Figure 6B). In contrast, the development of RPE was clearly delayed in CuONP-treated embryos, with 61.4% of embryos showing significantly reduced pigmentation accumulated in the RPE (Figure 6C). This result suggests that CuONP may selectively

https://dx.doi.org/10.1021/acsami.0c11052
ACS Appl. Mater. Interfaces 2020, 12, 50203−50211

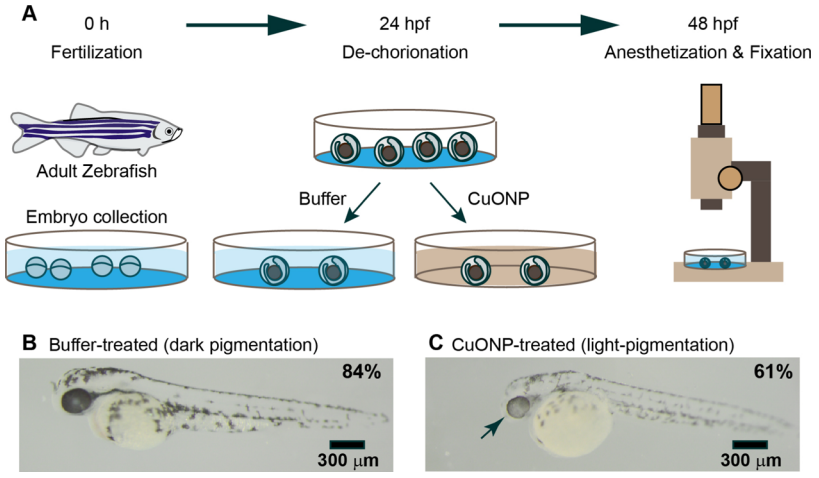

Figure 6. Characterization of the cytotoxicity of purified CuONP to zebrafish embryos. (A) Schematic depicting the determination of CuONP on the embryonic developmental process of zebrafish. Hours post fertilization, hpf. (B) Representative image of wild-type AB strain embryos incubated in buffer at 48 hpf. The majority (84%) of embryos show normal dark pigmentation across the body. The number of embryos examined, 49. (C) Representative image of identical AB strain treated with 85 ppm of purified CuONP at 48 hpf. The majority (61%) of embryos show significantly reduced pigmentation across the body, in particular around the retina pigmented epithelium (arrow). The number of embryos examined, 57.

affect specific cell types during early vertebrate development, likely related to the oxidative stress that CuONP induced in developing embryos.

With growing production and applications of nanometer-sized materials, considerations should be taken so that the nanoparticle material is safe for use and, of arguably equal importance, can safely be disposed of. While many nanoparticles are tested for human contacts, such as in wound healing agents,[34−36] food,[37−39] sunscreens,[40] disinfectants,[41] and biosensors for drug delivery,[37] many are produced with little or no information about their biocompatibility.[42] Furthermore, it is also not always required to disclose nanoparticles as ingredients.[43]

Here, we focused on copper/copper oxide nanoparticles, which are used as "catalysts, magnetic storage media, solar energy transformers, solar cells, lithium batteries, semiconductors, field emission devices, gas sensors, biosensors in drug delivery, electronic chips, and heat transfer nanofluids".[37] Increasing research is being done to understand and manage the risks to the food chains, aquatic ecosystems, and microorganisms.[40,44,45] However, a comparative study on the cytotoxicity of copper nanoparticles in prokaryotic and eukaryotic cells is not available.

We used a protocol based on an environmentally friendly synthetic route for copper (oxide) nanoparticles to produce sub-10 nm copper nanoparticles.[22] This synthetic route utilizes L-ascorbic acid (vitamin C) and copper chloride with no extreme pressures or temperatures. This promising synthesis is one of the growing collection of green synthesis techniques.[46] We further characterized the biocompatibility of these nanoparticles to gain insight into their applications as well as to assess their potential risks. The size of our synthesized nanoparticles was slightly larger than 2 nm but still sub-10 nm, which may result from different heating methods.

Our results indicate that the residual reactants, particularly L-ascorbic acid, in the solution can contribute to some of the toxicity (Figure 3). To determine the contribution of death directly from the nanoparticles, we purified the sub-10 nm nanoparticles using gel electrophoresis. We found that the minimal inhibitory concentrations for purified nanoparticles in were 170 ppm in bacteria and 122.5 ppm in human cells (Figure 5), respectively. To further determine the cytotoxicity of the sub-10 nm copper particle for living organisms, we probed the effect of purified CuONP on the developmental process of zebrafish embryos. At 85 ppm, we found that CuONP significantly reduced the pigmentation of the embryos, particularly at the retina pigmented epithelium. Ongoing efforts aim to further determine the effect of surface bioconjugation on the cytotoxicity of sub-10 nm copper nanoparticles.

CONCLUSIONS

In this work, we carried out a comparative study to determine the biological effects of sub-10 nm copper nanoparticles on biological systems such as bacteria, yeast, mammalian cell lines, and live zebrafish embryos. Using cell viability and embryological assays, we determined that the safe concentration threshold for purified nanoparticle is approximately 85 ppm. Above this threshold, sub-10 nm copper particles inhibit the growth of bacteria and yeast, induce mammalian cell death, and cause developmental defects in the pigmentation of retina pigmented epithelium in zebrafish embryos. The result of cytotoxicity of CuONP to the tested prokaryotic and eukaryotic systems suggests that caution should be used to avoid direct contact of copper nanoparticles to human tissues considering the potential use of copper nanoparticles in the clinical setting.

EXPERIMENTAL SECTION

Synthesis of Copper Oxide Nanoparticles. Copper oxide nanoparticles (CuONPs) were synthesized using the Wu group's method[22] with some modifications. First, 5 mL of 600 mM L-ascorbic acid was heated to 80 °C and then 5 mL of 10 mM $CuCl_2$ was added dropwise to the magnetically stirred L-ascorbic solution. The mixture was then transferred to a capped bottle and put in an MTI gravity convection oven (Cat. #: DMG-9015) at 80 °C for 22 h.

The resulting CuONP solution was centrifuged twice at 4900 *g* for 10 min in a Sorvall ST 16R Centrifuge. The supernatant was collected with a BD 10 mL syringe (Cat. #: 300912) and filtered through a Millex syringe-driven filter unit of 0.22 μm from Merck Millipore (Cat. #: SLMP025SS). CuONPs were stored in a capped bottle at

https://dx.doi.org/10.1021/acsami.0c11052
ACS Appl. Mater. Interfaces 2020, 12, 50203−50211

room temperature in the dark. The w/w concentration of unpurified stock copper nanoparticle was estimated by assuming a complete reaction, which resulted in a concentration of 3 mg (Cu)/10 mL (solution) or 300 ppm (w/w).

UV Spectroscopy. Solutions of 600 mM L-ascorbic acid, 10 mM $CuCl_2$, and 600 mM L-ascorbic acid + 10 mM $CuCl_2$ were left in an MTI convection oven for a period of 22 h. The resulting L-ascorbic acid, $CuCl_2$, and CuONP solutions were calibrated using a NanoDrop) Spectrophotometer (ND2000C, Thermo Scientific). The L-ascorbic acid solution and $CuCl_2$ solution were measured at 600, 300, and 150 mM and 10, 5, and 2.5 mM, respectively.

Infrared Spectroscopy. Synthesized nanoparticles were characterized by IR. Both the CuONP solution and the unreacted 600 mM L-ascorbic acid spectrum were obtained using a PerkinElmer Spectrum Two FT-IR.

Transmission Electron Microscopy. Electron microscopy data collection was done with the help of staff from the University of Illinois at Urbana Champaign on a JOEL2200FS TEM microscope using graphene oxide on Quantifoil R2/4 200 grid mesh Cu grids (Cat. #: 4510C-BA, Structure Probe Inc.). Sample preparation followed a previous protocol using ultrasonic nebulization.[47]

Isolating CuONPs Using Gel Electrophoresis. An agarose gel was made by mixing 2 g of agarose with 100 mL of 40 mM Tris-acetate solution not containing ethylenediaminetetraacetic acid (EDTA) (TA buffer). Two gel combs were placed about 2 cm apart in the gel until solidified. After covering gel with TA buffer, 75 μL of CuONP solution was added to each of the wells in the set closest to the anode. The gel was then run at 140 mV until the CuONPs reached the set of wells closest to the cathode. Then, 100 μL of solution was collected from each well. To ensure that as many CuONPs were recovered as possible, the agarose gel was run for an additional 30 s and 100 μL was collected from every well in the set closest to the cathode. This process was repeated until all CuONPs were collected and pooled. The CuONPs solution was then transferred to a 1.5 mL vial, and the liquid was removed by a rotary evaporator. The dry CuONPs were then weighed and dissolved in DEPC-treated water. Considering the salt in the TA buffer will also contribute to the dry weight, we used the initial reactant $CuCl_2$ to estimate the final concentration of CuONP particles assuming a complete reaction. A 10 mL of crude CuONP was estimated to produce 1.6 mL of 2.0 mg/mL (2000 ppm, w/w) of purified particles. This stock was then diluted to produce the final concentration used in cell- and zebrafish-based assays.

Dynamic Light Scattering and ζ-Potential Measurements. Purified CuONP was diluted to different concentrations in the nanopure water from the stock solution. Dynamic light scattering and ζ-potential measurements were performed with a Malvern Zetasizer NanoZs using purified nanoparticles. Data analysis was performed using Malvern Zetasizer software.

Bacterial and Yeast Growth. *E. coli* (Stellar Cells, CAT) was grown and transformed with a pCS2 plasmid containing EGFP and ampicillin resistance. These cells were grown in Lennox broth containing ampicillin to log phase to make a starter culture. Each biological replicate came from a new starter culture from the same bacterial stock. From this starter culture, cells were added to culture tubes with freshly autoclaved LB + ampicillin to a final optical density at 600 nm of 0.1. Dose-dependent purified CuONPs in the TA buffer were used for cell treatment, whereas an equal volume of TA buffer alone was used as a control. Bacteria were incubated for 18 h. The optical density at 600 nm was measured either continuously via a BioTek Synergy H4 Hybrid Multi-Mode Microplate Reader or Nanodrop before and after incubation for endpoint experiments.

The *S. cerevisiae* (BJ3505 strain) cells[48] were grown at 30 °C overnight in YPD media with ampicillin. From this starter culture, cells were diluted into fresh YPD media containing copper nanoparticles in 96-well plates. Cells were grown at 30 °C in a plate reader with constant shaking for 18 h before OD at 600 nm was measured. YPD media contains 10 g/L yeast extract, 20 g/L peptone, and 20 g/L dextrose.

Determining Bacterial Colony-Forming Units (CFUs). After incubation for 18 h and growth measurement at OD of 600 nm, cells from each condition were diluted 1:10^6 in the LB broth. Then, 10 μL of diluted cells were pipetted on a marked agar plate and incubated 20 h at 37 °C in a VWR incubator.

CuONP Treatment of HEK293T Cells. In a 24-well plate, HEK293T were treated with Dulbecco's modified Eagle's medium (DMEM, Cat. #: 11995040, Thermo Fisher) + 10% fetal bovine serum (FBS, Cat. #: 12303C-500 mL, Sigma-Aldrich), containing CuONP at 8.5, 42.5, 85, 122.5, and 170 ppm or, as a control, an equal volume of TA buffer. To determine toxicity, copper nanoparticles or TA-containing media were removed and replaced with DMEM + 10% FBS containing calcein-AM (Cat. #: C3100MP, Thermo Fisher) and propidium iodide (PI, Cat. #: P1304MP, Thermo Fisher) and incubated as recommended in manufacturer's instructions. The calcein-AM and PI stain-treated cells were imaged using an epi-illumination microscope (DMi8, Leica) equipped with LAS X software. Analysis and quantification were performed using FIJI software.

MTS Assay. The CellTiter 96 AQueous One Solution Cell Proliferation Assay (100 μL, Cat. #: G3580, Promega) was added to each well of a 24-well plate. The plate was then placed in an incubator at 37 °C, 5% CO_2, for 1 h according to the manufacturer's protocol. The OD of the wells at 495 nm was measured using the Biotek Synergy H4 Hybrid Multi-Mode Microplate Reader.

CuONP Treatment of Zebrafish Embryos. The cleavage-stage zebrafish (*Danio rerio*) embryos were collected from the breeding setup between wild-type AB line zebrafish parents 0.5−1 h post fertilization (hpf). At 24 hpf, embryos were dechorionated and were grown in 1× E3 media with methylene blue (untreated control) or were treated with 85 ppm CuONP (diluted in the same E3 medium). At 24−30 h post-treatment, the embryos were fixed with 4% paraformaldehyde in 1× phosphate buffer saline (PBS) for 1 h, followed by thorough rinsing with 1× PBS. 1× E3 medium was diluted from the 60× stock that is made by dissolving 17.52 g of NaCl, 0.76 g of KCl, 2.92 g of $CaCl_2 \cdot H_2O$, and 4.88 g of $MgSO_4 \cdot 7H_2O$ in water. To every 1 L of 1× E3, 1 mL of 0.01% methylene blue was added to prevent fungal growth. Embryos were imaged using an Olympus XC30 camera and the cellSens application. All experimental procedures on zebrafish embryos were approved by the Illinois Institutional Animal Care and Use Committee (IACUC).

■ ASSOCIATED CONTENT

Supporting Information

The Supporting Information is available free of charge at https://pubs.acs.org/doi/10.1021/acsami.0c11052.

Calibration of the concentration of the remnant $CuCl_2$ reactant, CuONP induced oxidative stress in HEK293T cells, hydrodynamic radius of purified CuONP, and ζ-potential and conductivity of purified CuONP (PDF)

■ AUTHOR INFORMATION

Corresponding Author

Kai Zhang − *Department of Biochemistry, School of Molecular and Cellular Biology, University of Illinois at Urbana-Champaign, Urbana, Illinois 61801, United States*; Email: kaizkaiz@illinois.edu

Authors

Savanna S. Skeeters − *Department of Biochemistry, School of Molecular and Cellular Biology, University of Illinois at Urbana-Champaign, Urbana, Illinois 61801, United States*

Ana C. Rosu − *Department of Biochemistry, School of Molecular and Cellular Biology, University of Illinois at Urbana-Champaign, Urbana, Illinois 61801, United States*

https://dx.doi.org/10.1021/acsami.0c11052
ACS Appl. Mater. Interfaces 2020, 12, 50203−50211

Divyanshi − *Department of Cell and Developmental Biology, School of Molecular and Cellular Biology, University of Illinois at Urbana-Champaign, Urbana, Illinois 61801, United States*
Jing Yang − *Department of Comparative Biosciences, University of Illinois at Urbana-Champaign, Urbana, Illinois 61802, United States*

Complete contact information is available at: https://pubs.acs.org/10.1021/acsami.0c11052

Author Contributions

A.C.R. synthesized the CuONPs and developed methods for isolating them. S.S.S. and K.Z. conceived the experimental design for measuring toxicity in bacteria, yeast, and HEK293T and prepared the figures. Divyanshi, K.Z., and J.Y. conceived the experimental design for the fish embryological assay. S.S.S., A.C.R., and Divyanshi conducted the experiments. S.S.S., A.C.R., and K.Z. prepared the manuscript. All authors have given approval to the final version of the manuscript.

Funding

This work is supported by the Westcott Bioscience Fellowship from the Department of Biochemistry at UIUC (S.S.S.) and NIH grants R35GM131810 (J.Y.) and R01GM132438 (K.Z.).

Notes

The authors declare no competing financial interest.

■ ACKNOWLEDGMENTS

A.C.R. thanks David Bergandine (University Laboratory High School, Urbana, IL) for his mentorship. S.S.S. thanks Prof. Catherine Murphy and the lab members (UIUC) for their insight and recommendations and the staff at MRL (UIUC) for assistance with TEM. The authors also thank Prof. Tobias Meyer (Stanford University) for the gift of PC12 NS1 cells, Prof. Lin-Feng Chen (UIUC) for the gift of HEK293T cells, and Prof. Rutilio Fratti (UIUC) for the gift of yeast strains.

■ ABBREVIATIONS

CuONPs, copper/copper oxide nanoparticles
calcein-AM, calcein-acetoxymethyl
FT-IR, Fourier transform infrared
HEK293T, human embryonic kidney 293T
PC12, adrenal phaeochromocytoma
PI, propidium iodide
TEM, transmission electron microscopy

■ REFERENCES

(1) Gawande, M. B.; Goswami, A.; Felpin, F. X.; Asefa, T.; Huang, X.; Silva, R.; Zou, X.; Zboril, R.; Varma, R. S. Cu and Cu-Based Nanoparticles: Synthesis and Applications in Catalysis. *Chem. Rev.* **2016**, *116*, 3722−3811.
(2) Han, Y.; Zhang, F.; Gong, H.; Cai, C. Double G-quadruplexes in a copper nanoparticle based fluorescent probe for determination of HIV genes. *Microchim. Acta* **2018**, *186*, No. 30.
(3) Chen, C.; Geng, F.; Wang, Y.; Yu, H.; Li, L.; Yaang, S.; Liu, J.; Huang, W. Design of a nanoswitch for sequentially multi-species assay based on competitive interaction between DNA-templated fluorescent copper nanoparticles, Cr^{3+} and pyrophosphate and ALP. *Talanta* **2019**, *205*, No. 120132.
(4) Chawla, S.; Rawal, R.; Pundir, C. S. Fabrication of polyphenol biosensor based on laccase immobilized on copper nanoparticles/chitosan/multiwalled carbon nanotubes/polyaniline-modified gold electrode. *J. Biotechnol.* **2011**, *156*, 39−45.
(5) Solairaj, D.; Rameshthangam, P.; Muthukumaran, P.; Wilson, J. Studies on electrochemical glucose sensing, antimicrobial activity andcytotoxicity of fabricated copper nanoparticle immobilized chitinnanostructure. *Int. J. Biol. Macromol.* **2017**, *101*, 668−679.
(6) Ibupoto, Z. H.; Khun, K.; Beni, V.; Liu, X.; Willander, M. Synthesis of novel CuO nanosheets and their non-enzymatic glucose sensing applications. *Sensors* **2013**, *13*, 7926−7938.
(7) Wang, Z.; Wang, Z.; Lu, W. W.; Zhen, W.; Yang, D.; Peng, S. Novel biomaterial strategies for controlled growth factor delivery for biomedical applications. *NPG Asia Mater.* **2017**, *9*, No. e435.
(8) Sharma, A. K.; Kumar, A.; Sahu, M.; Sharma, G.; Datusalia, A. K.; Rajput, S. K. Exercise Preconditioning and Low Dose Copper Nanoparticles Exhibits Cardioprotection Through Targeting GSK-3β Phosphorylation in Ischemia:Reperfusion Induced Myocardial Infarction. *Microvasc. Res.* **2018**, *120*, 56−66.
(9) Cholewińska, E.; Ognik, K.; Fotschki, B.; Zdunczyk, Z.; Juskiewicz, J. Comparison of the effect of dietary copper nanoparticles and one copper (II) salt on the copper biodistribution and gastrointestinal and hepatic morphology and function in a rat model. *PLoS One* **2018**, *13*, No. e0197083.
(10) Arancibia, S.; Barrientos, A.; Torrejón, J.; Escobar, A.; Beltrán, C. J. Copper oxide nanoparticles recruit macrophages and modulate nitric oxide, proinflammatory cytokines and PGE2 production through arginase activation. *Nanomedicine* **2016**, *11*, 1237−1251.
(11) Perde-Schrepler, M.; Florea, A.; Brie, I.; Virag, P.; Fischer-Fodor, E.; Vâlcan, A.; Gurzău, E.; Lisencu, C.; Maniu, A. Size-Dependent Cytotoxicity and Genotoxicity of Silver Nanoparticles in Cochlear Cells In Vitro. *J. Nanomater.* **2019**, *2019*, No. 6090259.
(12) Korshed, P.; Li, L.; Liu, Z.; Mironov, A.; Wang, T. Size-dependent antibacterial activity for laser-generated silver nanoparticles. *J. Interdiscip. Nanomed.* **2019**, *4*, 24−33.
(13) Yoon, K. Y.; Byeon, J. H.; Park, J. H.; Hwang, J. Susceptibility constants of *Escherichia coli* and *Bacillus subtilis* to silver and copper nanoparticles. *Sci. Total Environ.* **2007**, *373*, 572−575.
(14) Azam, A.; Ahmed, A. S.; Oves, M.; Khan, M. S.; Habib, S. S.; Memic, A. Antimicrobial activity of metal oxide nanoparticles against Gram-positive and Gram-negative bacteria: a comparative study. *Int. J. Nanomed.* **2012**, *7*, 6003−6009.
(15) Ashajyothi, C.; Harish, K. H.; Dubey, N.; Chandrakanth, R. K. Antibiofilm activity of biogenic copper and zinc oxide nanoparticles-antimicrobials collegiate against multiple drug resistant bacteria: a nanoscale approach. *J. Nanostruct. Chem.* **2016**, *6*, 329−341.
(16) Rodhe, Y.; Skoglund, S.; Wallinder, I. O.; Potacova, Z.; Moller, L. Copper-based nanoparticles induce high toxicity in leukemic HL60 cells. *Toxicol. In Vitro* **2015**, *29*, 1711−1719.
(17) McLean, R. J. C.; Hussain, A. A.; Sayer, M.; Vincent, P. J.; Hughes, D. J.; Smith, T. J. N. Antibacterial activity of multilayer silver−copper surface films on catheter material. *Can. J. Microbiol.* **1993**, *39*, 895−899.
(18) Schmidt, M. G.; Attaway, H. H.; Sharpe, P. A.; John, J., Jr.; Sepkowitz, K. A.; Morgan, A.; Fairey, S. E.; Singh, S.; Steed, L. L.; Cantey, J. R.; Freeman, K. D.; Michels, H. T.; Salgado, C. D. Sustained reduction of microbial burden on common hospital surfaces through introduction of copper. *J. Clin. Microbiol.* **2012**, *50*, 2217−2223.
(19) Chatterjee, A. K.; Chakraborty, R.; Basu, T. Mechanism of antibacterial activity of copper nanoparticles. *Nanotechnology* **2014**, *25*, No. 135101.
(20) Vincent, M.; Duval, R. E.; Hartemann, P.; Engels-Deutsch, M. Contact killing and antimicrobial properties of copper. *J. Appl. Microbiol.* **2018**, *124*, 1032−1046.
(21) Shankar, S.; Teng, X.; Rhim, J.-W. Properties and characterization of agar:CuNP bionanocomposite filmsprepared with different copper salts and reducing agents. *Carbohydr. Polym.* **2014**, *114*, 484−492.
(22) Xiong, J.; Wang, Y.; Xue, Q.; Wu, X. Synthesis of highly stable dispersions of nanosized copper particles using l-ascorbic acid. *Green Chem.* **2011**, *13*, 900−904.
(23) Wang, C.; Wang, C.; Xu, L.; Cheng, H.; Lin, Q.; Zhang, C. Protein-directed synthesis of pH-responsive red fluorescent copper

nanoclusters and their applications in cellular imaging and catalysis. *Nanoscale* **2014**, *6*, 1775−1781.
(24) Wang, C.; Cheng, H.; Huang, Y.; Xu, Z.; Lin, H.; Zhang, C. Facile sonochemical synthesis of pH-responsive copper nanoclusters for selective and sensitive detection of Pb^{2+} in living cells. *Analyst* **2015**, *140*, 5634−5639.
(25) Hokita, Y.; Kanzaki, M.; Sugiyama, T.; Arakawa, R.; Kawasaki, H. High-Concentration Synthesis of Sub-10-nm Copper Nanoparticles for Application to Conductive Nanoinks. *ACS Appl. Mater. Interfaces* **2015**, *7*, 19382−19389.
(26) Wu, S. Preparation of fine copper powder using ascorbic acid as reducing agent and its application in MLCC. *Mater. Lett.* **2007**, *61*, 1125−1129.
(27) Chahdoura, F.; Pradel, C.; Gómez, M. Copper(I) Oxide Nanoparticles in Glycerol: A Convenient Catalyst for Cross-Coupling and Azide−Alkyne Cycloaddition Processes. *ChemCatChem* **2014**, *6*, 2929−2936.
(28) Zhang, J.; Wang, J.; Fu, Y.; Zhang, B.; Xie, Z. Sonochemistry-synthesized CuO nanoparticles as an anode interfacial material for efficient and stable polymer solar cells. *RSC Adv.* **2015**, *5*, 28786−28793.
(29) Sehmi, S. K.; Noimark, S.; Weiner, J.; Allan, E.; MacRobert, A. J.; Parkin, I. P. Potent Antibacterial Activity of Copper Embedded into Silicone and Polyurethane. *ACS Appl. Mater. Interfaces* **2015**, *7*, 22807−22813.
(30) Song, L.; Connolly, M.; Fernandez-Cruz, M. L.; Vijver, M. G.; Fernandez, M.; Conde, E.; de Snoo, G. R.; Peijnenburg, W. J.; Navas, J. M. Species-specific toxicity of copper nanoparticles among mammalian and piscine cell lines. *Nanotoxicology* **2014**, *8*, 383−393.
(31) Lemire, J. A.; Harrison, J. J.; Turner, R. J. Antimicrobial activity of metals: mechanisms, molecular targets and applications. *Nat. Rev. Microbiol.* **2013**, *11*, 371−384.
(32) Claridge, S. A.; Liang, H. W.; Basu, S. R.; Frechet, J. M.; Alivisatos, A. P. Isolation of discrete nanoparticle-DNA conjugates for plasmonic applications. *Nano Lett.* **2008**, *8*, 1202−1206.
(33) Parak, W. J.; Pellegrino, T.; Micheel, C. M.; Gerion, D.; Williams, S. C.; Alivisatos, A. P. Conformation of Oligonucleotides Attached to Gold Nanocrystals Probed by Gel Electrophoresis. *Nano Lett.* **2003**, *3*, 33−36.
(34) Alizadeh, S.; Seyedalipour, B.; Shafieyan, S.; Kheime, A.; Mohammadi, P.; Aghdami, N. Copper nanoparticles promote rapid wound healing in acute full thickness defect via acceleration of skin cell migration, proliferation, and neovascularization. *Biochem. Biophys. Res. Commun.* **2019**, *517*, 684−690.
(35) Rakhmetova, A. A.; Alekseeva, T. P.; Bogoslovskaya, O. A.; Leipunskii, I. O.; Ol'khovskaya, I. P.; Zhigach, A. N.; Glushchenko, N. N. Wound-healing properties of copper nanoparticles as a function of physicochemical parameters. *Nanotechnol. Russia* **2010**, *5*, 271−276.
(36) Tao, B.; Lin, C.; Deng, Y.; Yuan, Z.; Shen, X.; Chen, M.; He, Y.; Peng, Z.; Hu, Y.; Cai, K. Copper-nanoparticle-embedded hydrogel for killing bacteria and promoting wound healing with photothermal therapy. *J. Mater. Chem. B* **2019**, *7*, 2534−2548.
(37) Maharramov, A. M.; Hasanova, U. A.; Suleymanova, I. A.; Osmanova, G. E.; Hajiyeva, N. E. The engineered nanoparticles in food chain: potential toxicity and effects. *SN Appl. Sci.* **2019**, *1*, No. 1362.
(38) Carrillo-Inungaray, M. L.; Trejo-Ramirez, J. A.; Reyes-Munguia, A.; Carranza-Alvarez, C. Use of Nanoparticles in the Food Industry: Advances and Perspectives. In *Impact of Nanoscience in the Food Industry*; Academic Press, Cambridge, MA, 2018; pp 419−444.
(39) Singh, T.; Shukla, S.; Kumar, P.; Wahla, V.; Bajpai, V. K.; et al. Application of Nanotechnology in Food Science: Perception and Overview. *Front. Microbiol.* **2017**, *8*, No. 1501.
(40) Heiligtag, F. J.; Niederberger, M. The fascinating world of nanoparticle research. *Mater. Today* **2013**, *16*, 262−271.
(41) Rogers, K. R.; Navratilova, J.; Stefaniak, A.; Bowers, L.; Knepp, A. K.; Al-Abed, S. R.; Potter, P.; Gitipour, A.; Radwan, I.; Nelson, C.; Bradham, K. D. Characterization of engineered nanoparticles in commercially available spray disinfectant products advertised to contain colloidal silver. *Sci. Total Environ.* **2018**, *619−620*, 1375−1384.
(42) Khan, I.; Saeed, K.; Khan, I. Nanoparticles: Properties, applications and toxicities. *Arab. J. Chem.* **2019**, *12*, 908−931.
(43) Duncan, T. V. The communication challenges presented by nanofoods. *Nat. Nanotechnol.* **2011**, *6*, 683−688.
(44) Chang, Y.-N.; Zhang, M.; Xia, L.; Zhang, J.; Xing, G. The Toxic Effects and Mechanisms of CuO and ZnO Nanoparticles. *Materials* **2012**, *5*, No. 2850.
(45) Gupta, Y. R.; Sellegounder, D.; Kannan, M.; Deepa, S.; Senthilkumaran, B.; Basavaraju, Y. Effect of copper nanoparticles exposure in the physiology of the common carp (*Cyprinus carpio*) − Biochemical, histological and proteomic approaches. *Aquacult. Fish.* **2016**, *1*, 15−23.
(46) Singh, J.; Kaur, J.; Rawat, M. A Brief Review on Synthesis and Characterization of Copper Oxide Nanoparticles and its Applications. *J. Bioelectron. Nanotechnol.* **2016**, *1*, No. 9.
(47) Hinman, J. G.; Hinman, J. J.; Janicek, B. E.; Huang, P. Y.; Suslick, K. S.; Murphy, C. J. Ultrasonic Nebulization for TEM Sample Preparation on Single-Layer Graphene Grids. *Nano Lett.* **2019**, *19*, 1938−1943.
(48) Jones, E. W.; Zubenko, G. S.; Parker, R. R. Pep4 gene function is required for expression of several vacuolar hydrolases in *Saccharomyces cerevisiae*. *Genetics* **1982**, *102*, 665−677.

https://dx.doi.org/10.1021/acsami.0c11052
ACS Appl. Mater. Interfaces 2020, 12, 50203−50211